Pergamon

Journal of Structural Geology, Vol. 17, No. 8, pp. 1151 to 1163, 1995

0191-8141/95 $9.50+0.00

0191-8141(95)00015-1

Modes of reverse reactivation of domino-type normal faults: experimental and theoretical approach

NIBIR MANDAL and ANUPAM CHATTOPADHYAY

Department of Geological Sciences, Jadavpur University, Calcutta 700032, India

(*Received* 12 *January* 1994; *accepted in revised form* 4 *January* 1995)

Abstract—Experiments with sand–cement models show that reverse reactivation of a set of parallel faults bounding domino blocks takes place in two principal modes. In (Mode I) reactivation, the domino blocks undergo counter-rotation during contraction while normal faults are reactivated as reverse faults. Mode II reactivation occurs by fault-block translation. We present a theoretical analysis of the two modes which considers forces and their rotational moments in a domino block and show that low-angle normal faults are commonly reactivated in Mode II. By contrast, steep faults are reactivated in Mode I. Furthermore, fault reactivation depends on the initial fault spacing. A large initial fault spacing opposes fault reactivation, especially in Mode I. Instead, the system deforms along new thrusts, dipping opposite to the normal faults. We generate reactivation parameters for the conditions of the two modes as functions of the ratio (R) between fault spacing and effective thickness of fault horizon, the fault dip (θ), the coefficient of friction (μ) and the ratio of principal stresses (Sr) during late contraction.

INTRODUCTION

During inversion tectonics, regional contraction can reactivate pre-existing extensional faults as reverse faults (Cooper & Williams 1989, Williams *et al.* 1989, Letouzey *et al.* 1990) and the magnitude of reverse movement may reach several kilometers (Bruhn & Dalziel 1977). However, reverse reactivation may not take place in every domain of the thrust belt. Letouzey *et al.* (1990) have shown that reverse slip occurs along the deeper segments of the normal faults but not along shallower fault segments which typically dip more steeply. Experiments with analogue models (McClay 1989) also showed that reactivation of normal faults depends on their initial geometry and orientation with respect to the direction of later contraction. The location and orientation of new thrusts are also greatly controlled by pre-existing extensional faults (McClay & Buchanan 1991).

Low-angle normal faults have been found whose dips deviate significantly from those predicted by the Mohr–Coulomb criterion of failure (Doser 1987). Some of these faults are explained by reactivation of old thrusts or other planes of weakness during extension (Sykes 1978, Brewer & Smythe 1984, Smith & Bruhn 1984, Allmendinger *et al.* 1987, Enfield & Coward 1987).

There are some constraints in considering fault reactivation universal (Wernicke 1981, Wernicke *et al.* 1985, Etheridge 1986). Some field investigations (Hatcher 1981) have shown that many normal faults have not been reactivated, and that contraction is accommodated by new low-angle thrusts. Normal faults have been reactivated only in areas subjected to large extension prior to contraction (Etheridge 1986).

Theoretical analyses of fault reactivation (Etheridge 1986, Cèlèrier 1988, Ivins *et al.* 1990) show that the orientation of fault planes in the new stress system and the contrast in cohesive and frictional strengths between intact and previously faulted rocks are the principal parameters controlling fault reactivation. These parameters have a critical range of values in which reactivation is possible. Fluid pressure is another important parameter that may greatly enhance reactivation by lowering frictional resistance along the fault zone (Ivins *et al.* 1990).

In the present paper, we consider the reactivation of sets of parallel faults arranged in domino domains. Both experiments and theory indicate that the mode of reactivation depends on the fault arrangement, when all other physical factors are kept identical. Experiments also show that it is mechanically easier to reactivate parallel faults (dominos) than non-parallel fault arrays (horsts and grabens).

EXPERIMENTAL PROCEDURE

We modelled reverse reactivation of normal faults in experiments using weak, brittle sand–cement mixtures. Dry, fine-grained (65–70 mesh) white sand and white cement were mixed homogeneously in a 1:1 volume ratio. We generated layering by adding very small amounts of powders of different colours to the dry sand–cement mixture. This mixture was watered in sand–cement to water ratio 3:1 and became viscous. We then built sand–cement layers of different colours above a ductile base of painter's putty. The role of the basal ductile layer was to adjust and accommodate rigid displacements of fault blocks in the brittle bed during deformation. We used a very low viscosity (6.86×10^3 Pa s) putty so that the basal layer itself did not influence deformation in the brittle layer. The whole set-up rested on a rigid perspex plate. During model construction we kept glass plates on all four sides of the model to prevent

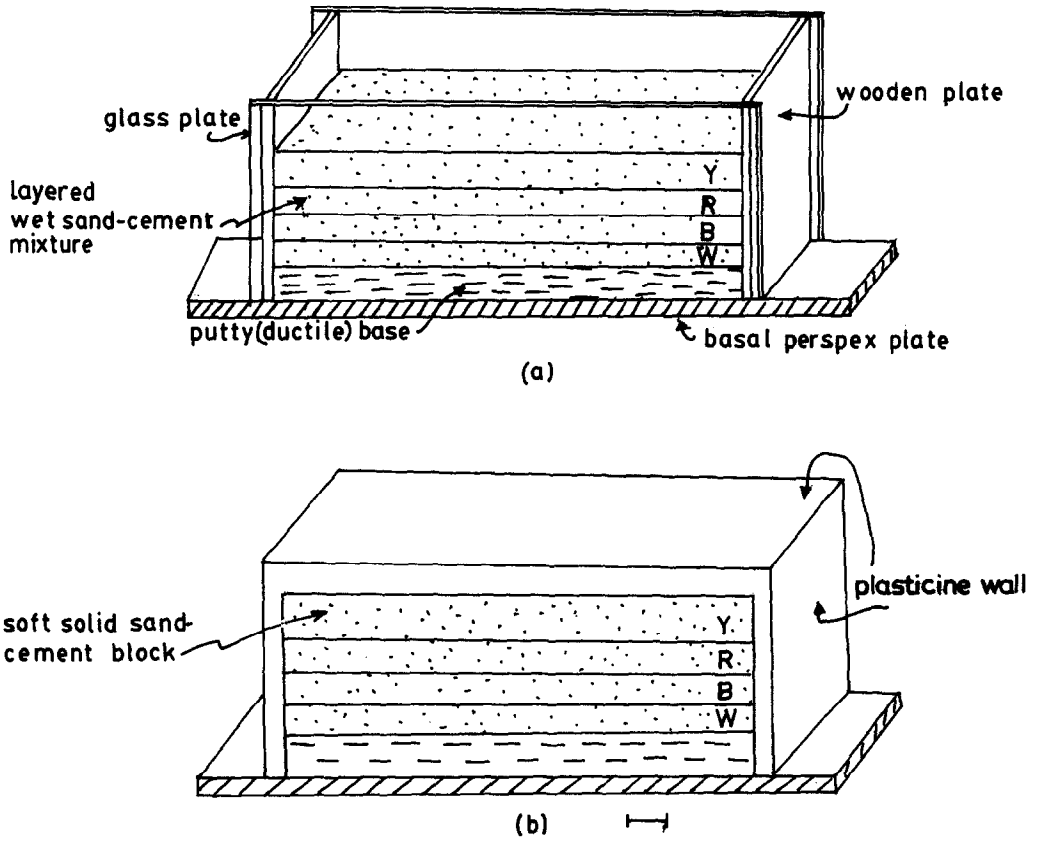

Fig. 1. (a) Schematic diagram of model preparation. (b) After removal of the boundary plates. Y: yellow; B: blue; R: red; W: white.

the viscous sand–cement mass from flowing (Fig. 1a). The model was then allowed to dry for about 20 minutes and to gain the cohesion of a weak solid. At this stage, the glass plates were removed without disturbing the model. Before starting deformation, the model was allowed to dry and strengthen for an additional 10 minutes. The two side walls and the top surface of the model were covered with soft plasticine (Fig. 1b). As the sand–cement mixture was cohesive, the models (25 cm × 12 cm × 5 cm) were not properly scaled to nature (see also Discussion). However, sand–cement beds were weak enough to fail under a load of 1450 Kg m^{-2}. The density of the sand–cement mixture was 2377 Kg m^{-3}.

Models were deformed in two steps. The model was first subjected to vertical compression in a pure-shear box (Fig. 2) which formed normal faults. The normal-faulted models were then deformed by horizontal contraction in a motor-driven pure-shear machine (Fig. 3). The contraction was normal to the strike of normal faults. Before beginning the second stage of deformation, we photographed the two lateral sides of the models to record the dips and offsets of the normal

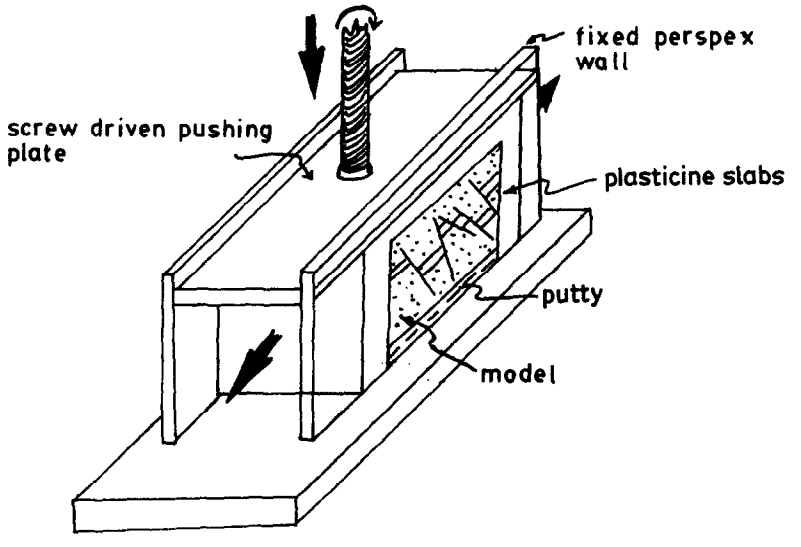

Fig. 2. First step of deformation (extension) of model in a pure-shear box.

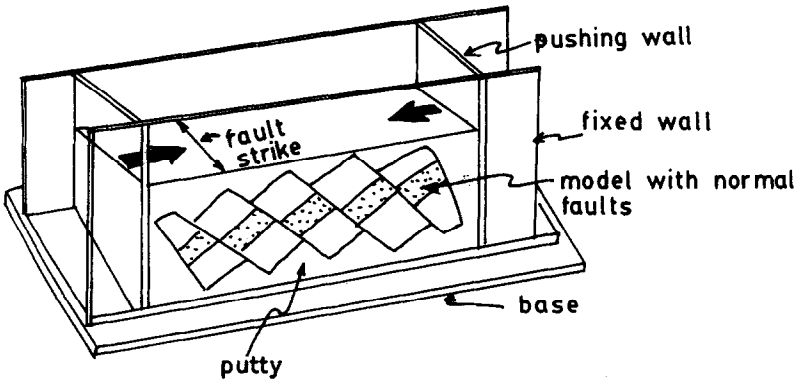

Fig. 3. Second step of deformation (contraction) of normal-faulted models in a motor-driven pure-shear machine.

faults. We observed and photographed successive stages of model deformation through the transparent perspex sidewalls.

EXPERIMENTAL RESULTS

Normal faults

Normal faults initiated with dips between 58° and 65°. They commonly formed in conjugate pairs, forming horst-and-graben structures (Fig. 7c,i). However, in some models we found domains of parallel faults bounding domino blocks. Typically, each model would have two domains of parallel faults with opposite vergence and a trapezoidal horst in the central part (Fig. 6a). We generated models with a single set of parallel faults in two ways. In the first method, a number of parallel cuts, with inclination equal to that of natural normal faults were first induced in the sand–cement bed at a desired spacing. When such a model was subjected to horizontal extension, these cuts were activated as normal faults bounding regularly spaced domino blocks (Fig. 4a). In the second method, similar to that of McClay & Ellis (1987) and Vendeville *et al.* (1987), we forced faults to form in a single set of parallel faults spontaneously, by tilting (dip of about 15°) the sand–cement bed (Fig. 4b). The normal faults had a uniform dip, synthetic of the slope of the sand–cement bed.

Reactivation of parallel normal faults

During later contraction, new thrusts did not form immediately in the domain of domino normal faults. There was reverse movement along the normal faults before the initiation of new low-angle thrusts at a late stage of contraction. The present series of experiments shows two modes of reverse reactivation which depend on dip and spacing of faults. In Mode I fault blocks undergo rigid rotation during the late contraction and pre-existing normal faults are reactivated as reverse faults (Fig. 5a). The normal faults progressively steepen passively by fault-block counter-rotation. Finite fault offsets and the dip of the layers progressively decrease with increasing contraction (Figs 5a and 6b). In Mode II, faults are reactivated in reverse movement without rigid block rotation (Fig. 5b). As a result, the dips of faults and layers do not change during contraction. Unlike Mode I reactivation, the layers remain tilted even after fault offsets vanish (5b and 6c,ii).

We conducted a set of experiments (Table 1) with normal faults dipping greater than 45°. In these experiments, horizontal extension formed normal faults, with initial dips of 60° and then rotated down to fault dips of about 56–48°. Later contraction caused reverse reactivation of the normal faults in Mode I. Finite offsets vanished when the layers and faults rotated back to their initial orientations. However, in most of the experiments, new thrusts formed prior to complete restoration of the fault offsets (Fig. 6b). Mode I reactivation in our experiments resemble the reactivation of extensional faults and the formation of new low-angle thrusts during inversion of rifted Brianconnais (figs. 13c & d, Butler 1989) and the External Crystalline Massifs in the Alps (fig. 9, Graciansky *et al.* 1989).

Pre-contraction fault spacing in models was a controlling factor in Mode I reactivation (Table 1). When fault spacing was very large (8.0 cm in a bed of 3.5 cm thickness), there was little or no reactivation and new low-angle thrusts formed in the early stage of contraction (Fig. 7b). In models with similar bed thickness but lower fault spacing (4.0 cm), faults were reactivated in Mode I during most of the contraction episode. New thrusts initiated only after the layers had rotated close to their initial position and the finite offsets reduced nearly to zero (Fig. 6b). In models with a much lower fault spacing (2.0 cm) reactivation was similar to that in the earlier case, but only every second fault in each domain was reactivated as reverse fault (Fig. 7a). Non-reactivated faults rotated passively and steepened during the reactivation by rigid-body rotation of fault blocks. The experiments thus indicate that reactivation of normal faults by counter-rotation of fault blocks is most effective for a critical fault spacing.

When the amount of early, horizontal extension was large, fault-block rotations greatly lowered the initial fault dip from 62° to less than 45° (Table 1). These gently dipping normal faults underwent Mode II reactivation in the early stage of contraction. As shortening progressed fault block rotation became more important and Mode I

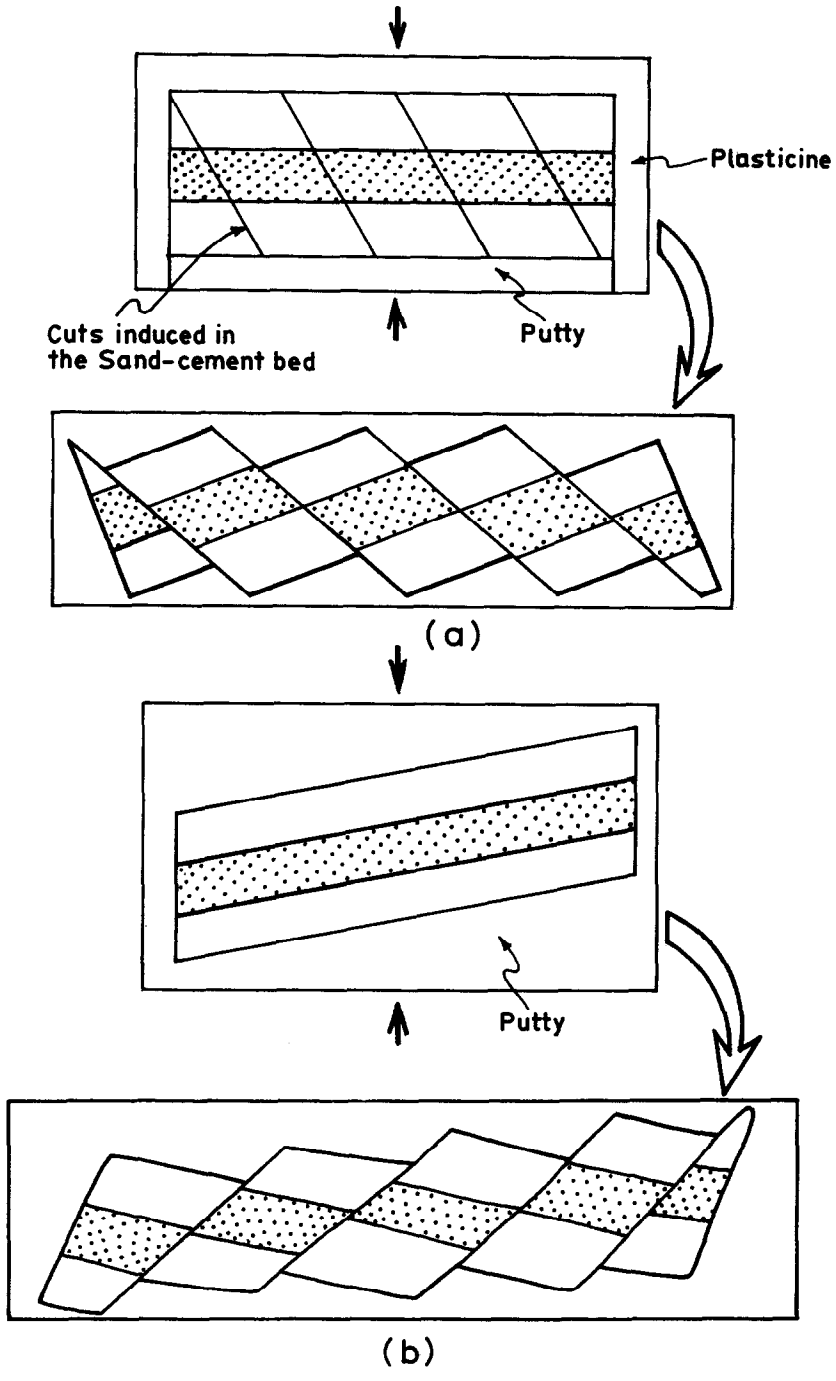

Fig. 4. Development of domino structures: (a) by activation of cuts induced in a horizontally deformed bed; and (b) by spontaneous formation of parallel faults in an inclined (dip = 15°) bed deformed under vertical compression.

reactivation dominated. In the advanced stages of contraction, reversal of fault offsets were obtained (Figs. 5c and 6c,iii). The inversion structure can be compared to reactivated normal fault systems in a continental collision zone (fig. 1, Butler 1989). Finally, new low-angle thrusts formed and the normal faults became passive.

Contraction of horst-and-graben structures

For the same physical conditions, late contraction did not reactivate normal faults significantly in horst-and-graben systems (Table 1). There was a small amount of homogeneous strain in the sand–cement bed that slightly steepened the normal faults but did not involve any slip on the normal faults. New low-angle thrusts appeared and cut across horst-and-graben structures before significant steepening of the normal faults (Fig. 7c,ii). The segmented horsts and grabens were transported by the new thrust and the normal faults remained inactive during the movement.

Development of new thrusts

In a large horizontal contraction domino normal faults steepened considerably and reverse slip on the normal faults decreased. It indicates that further shortening of the model by reactivation of the normal faults became increasingly difficult mechanically. At this stage, short-

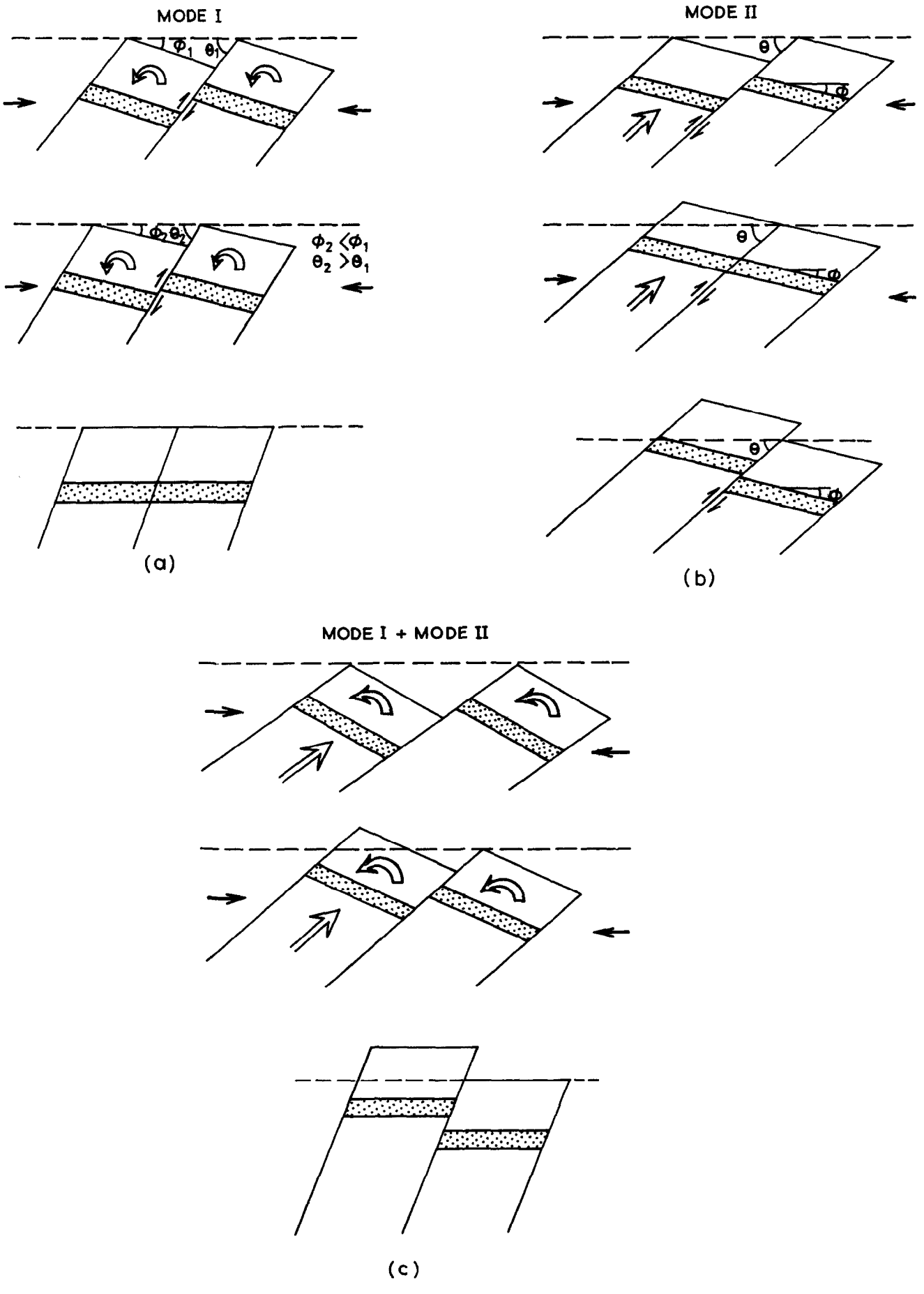

Fig. 5. Different modes of reverse reactivation of parallel normal faults. (a) Mode I, (b) Mode II, and (c) combination of Mode I and II.

Table 1. Summary of experimental results

Normal fault arrangement	Bed thickness (cm)	Fault spacing (cm)	Initial (pre-contraction) fault-dip (°)	Nature of reactivation	Fault-offset after contraction	Development of new thrusts
Parallel	(4) 3.5	8.0	52–56	Not significant	Unchanged	Early stage, vergence opposite to the normal faults
	(6) 3.5	4.0	49–54	Mode I	Decreased to almost zero	Late stage, vergence opposite to the normal faults
	(5) 3.5	2.0	48–52	Mode I selective reactivation of alternate faults	Non-uniform decrease in offset	Late stage, vergence opposite to the normal faults
	(4) 3.5	2.0	42–45	Mode II dominant in early stage, Mode I in late stage	Non-uniform offsets	Late stage thrusts, vergence opposite to the normal faults
	(6) 3.5	1.5	38–42	Mode II dominant, Mode I in very late stage	Reversal in offsets	Late stage thrusts
Non-parallel	(5) 4.0	—	58–63	Not significant	Unchanged	Early stage

Figures in parentheses indicate the number of experiments.

ening was accommodated by slip on new thrusts. The vergence of new thrusts in the domino structures was systematicaly opposite to that of the early set of parallel normal faults (Figs. 6b,ii and 7a,ii). This relationship between new thrusts and earlier normal faults consistently occurred in all experiments. Similar opposed vergence between new thrusts and normal faults is also found in inversion of natural half-graben systems, e.g. the Kechika Trough (fig. 11c, McClay *et al.* 1989). In some experiments, new thrusts formed along layer interfaces as bedding-thrusts. During normal faulting, layers rotated to dips close to that of potential plane of thrusting. Because there is an inherent mechanical weakness along layering, the new thrust propagated along the layer interfaces or cut it at a low-angle.

THEORETICAL ANALYSIS

Geometrical considerations

Let $T (=2t)$ be the vertical thickness of faulted horizon containing domino blocks and $L (= 2l)$ be the horizontal distance between two parallel normal faults F_1 and F_2 (Fig. 8). If δ is the displacement on the normal faults, then

$$h = t - \delta \sin \theta$$

where h is the vertical distance between the point P_2 and the center of the domino block (Fig. 8). θ is the fault dip. We consider two reference frames (oxy) and $(ox'y')$ at the center of the fault block with x and x'-axis parallel to the faulted horizon and the fault plane, respectively.

Criteria for Mode I reactivation

We consider rotational moments in the fault block for the analysis of Mode I reactivation. The rotational moment due to the normal component of traction, T to the fault face F_2 is M_d (equation A8). $T = \mathbf{F}$ ds, where $\mathbf{F}$ is stress vector (Muskhelisvili 1953). The rotational tendency due to M_d will be opposed by a moment, M_v (equation A9) due to the downward vertical forces. Then, the effective moment, M_r resultant of M_d and M_v induces a rotational motion in the block. Counter-rotation of the domino block may occur for positive values of M_r resulting in reactivation of the faults in Mode I. In equation (A10) M_r is a function of h, l, θ and S_r (σ_3/σ_1). With decreasing θ, M_r first increases gradually, then sharply decreases (Fig. 9). Thus Mode I can not be significant if normal faults initially have gentle dips. This theoretical inference conforms well with the experimental observations (Table 1). When h, θ and S_r are kept constant, there is a definite range of l values for which M_r is positive (Fig. 10). Thus, normal faults can be reactivated in Mode I for a specific range of initial fault spacing as found in the experiments.

In the range of positive values of M_r, rotational motion will occur in the block when M_r exceeds the resistive moment M_f (equation A12) due to friction along the faults. For example, M_r exceeds M_f at l = 1.6 cm for $\mu = 0.5$ (Fig. 10). Normal faults with lower spacing will not be reactivated in Mode I. Normal faults that are initially closely spaced can be selectively reactivated with a spacing for which $M_r > M_f$, as has been observed in the experiments (Fig. 7a). The threshold l-value below which Mode I is not favoured depends on the coefficient of friction (μ). For example, it is 1.1 when $\mu = 0.4$ and 2.0 when $\mu = 0.6$ (Fig. 10) for $h = 2$, $\theta = 50°$ and $S_r = 0.5$.

Criteria for Mode II reactivation

To analyze Mode II reactivation we consider the tangential component (F_t) of the traction (equation

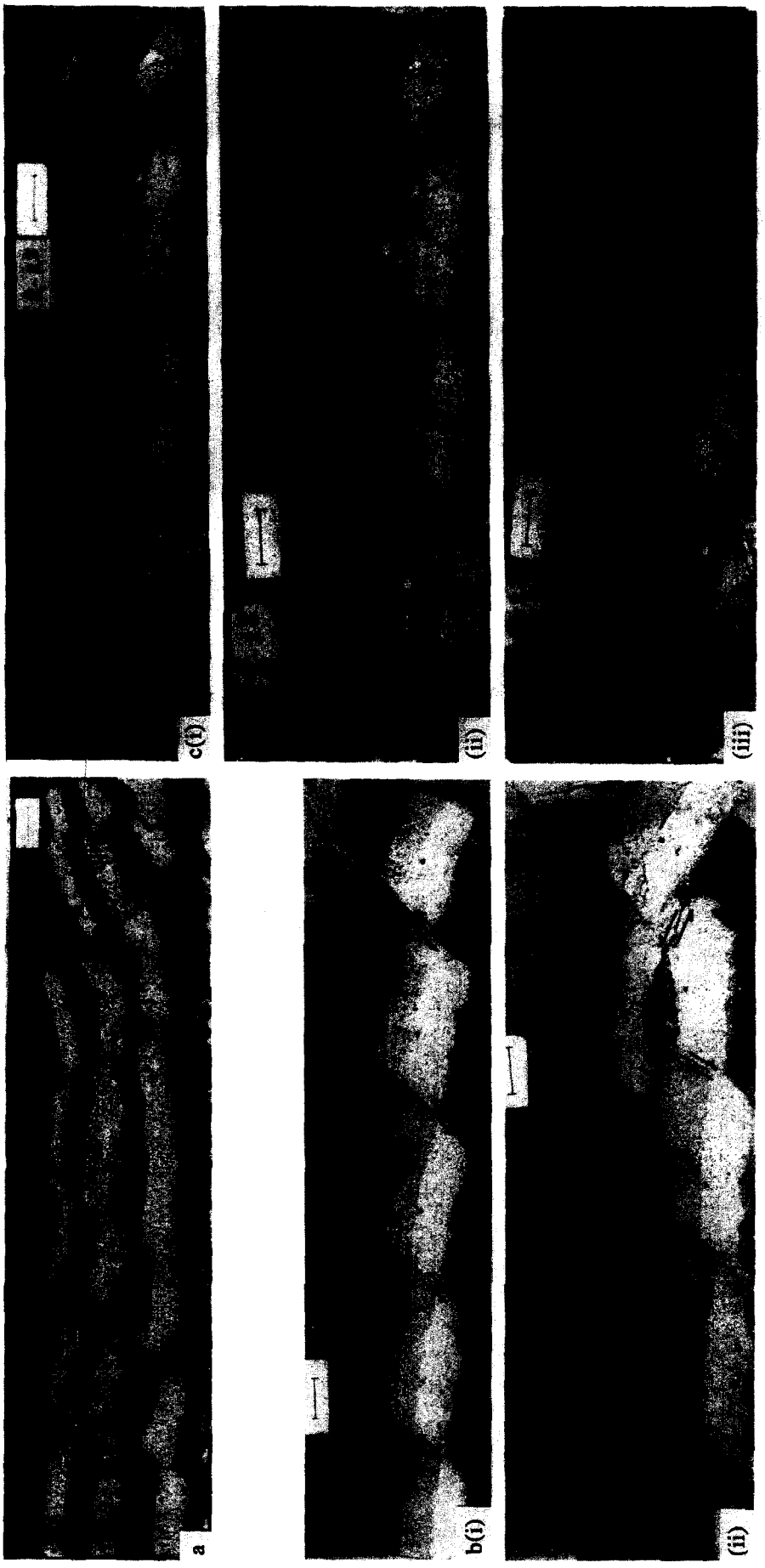

Fig. 6. (a) Development of two sets of oppositely dipping domino faults in sand–cement bed by early horizontal extension. (b) Mode I reactivation of normal faults, followed by initiation of a thrust after horizontal contraction: (i) after 8.23% extension; and (ii) after 15.23% contraction, the initial dip of normal faults was 49°. (c) Mode II reactivation: (i) after 36.1% extension; (ii) & (iii) after 15.4% and 24.7% shortening, respectively. Initial fault dip was 41°. Mode I became important at a later stage of contraction and steepened the faults.

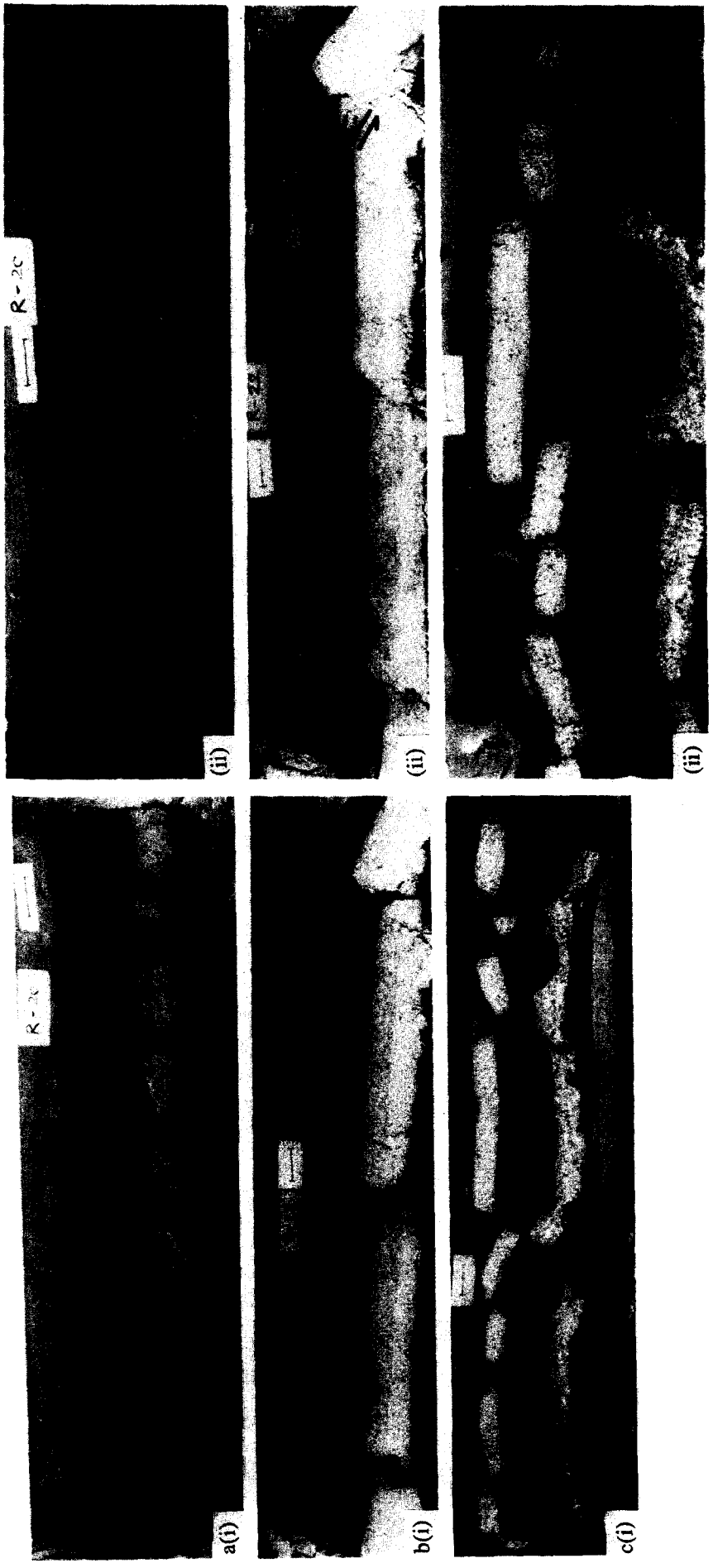

Fig. 7. (a) Selective reactivation in Mode I in a domino set, initial fault spacing 2 cm, bed thickness 3.7 cm and fault dip 52°: (i) after 12.1% extension; and (ii) after 14.23% shortening. (b) Formation of new thrust with no significant reactivation: initial fault spacing 8.0 cm, bed thickness 3.5 cm; (i) after 5.0% extension; and (ii) after 13.0% shortening. (c) Contraction of horst-and-graben structures. Note that new thrust formed without significant reactivation of earlier normal faults: (i) after 13.0% extension; and (ii) after 24.7% shortening.

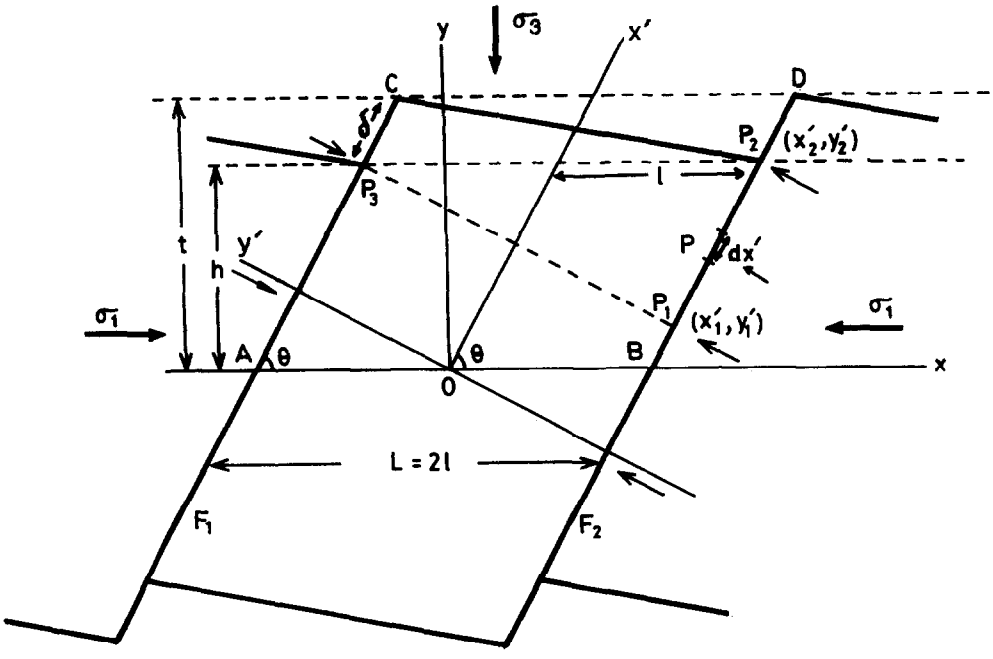

Fig. 8. Geometrical parameters and forces in a domino block (see text for details).

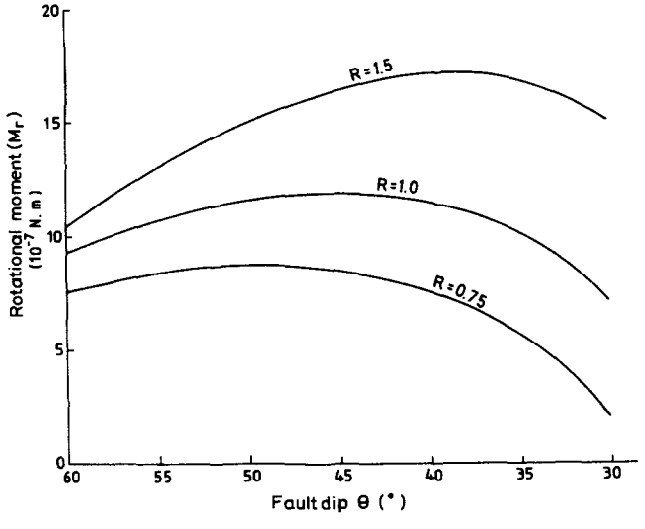

Fig. 9. Calculated plots of rotational moment (M_r) in a domino block vs initial fault dip (θ) for different R ($= l/h$) values.

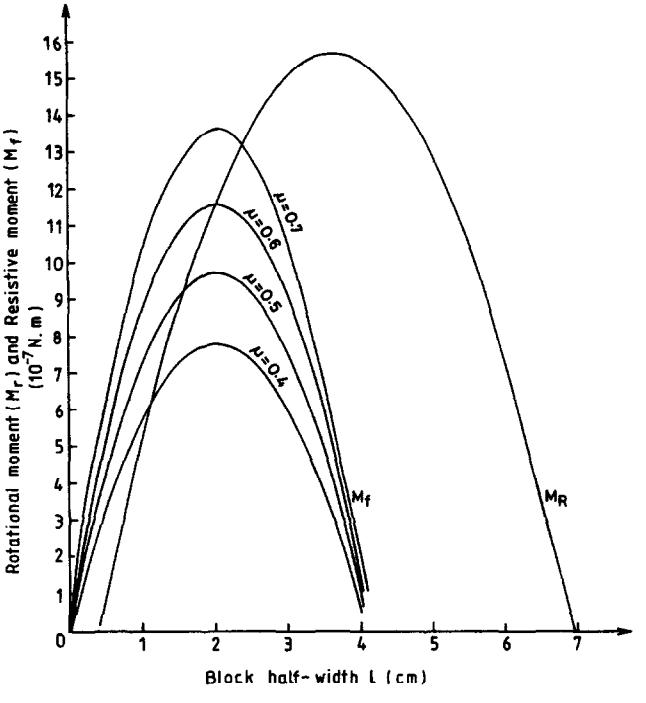

Fig. 10. Plots of rotational moment (M_r) and resistive moment (M_f) vs initial fault spacing (l) for different values of coefficient of friction (μ).

A14) to the fault. Block movement is opposed by the overburden load on the faulted horizon. The resultant force (F_θ) of these two forces F_t and F_d (equation A16) will impart a reverse slip on the faults. Reverse slip will be opposed by the frictional force (F_r) (equation A17). Mode II reactivation could occur for $F_\theta > F_r$. The theoretical curves for F_θ and F_r vs θ (Fig. 11) also indicate that Mode II is important when normal faults had gentle dips before contraction.

Reactivation parameters

From the above theoretical analysis we can define two parameters to express the critical conditions for the two modes of reactivation.

Mode I: the ratio between opposing and driving rotational moments is considered to generate reactivation parameter (α) as

$$\alpha = \phi_1 + \lambda\phi_2 \text{ where } \phi_1 = M_v/M_d \text{ and } \phi_2 = M_f/M_d \quad (1)$$

where λ is to be taken as 1 when ϕ_2 is positive. ϕ_2 may become negative as a consequence of geometrical construction in the present theoretical analysis. Because M_f cannot be negative, λ is to be taken 0 to nullify the second term in equation (1). Substituting ϕ_1 and ϕ_2 from equations (A18) and (A19) in equation (1) we get

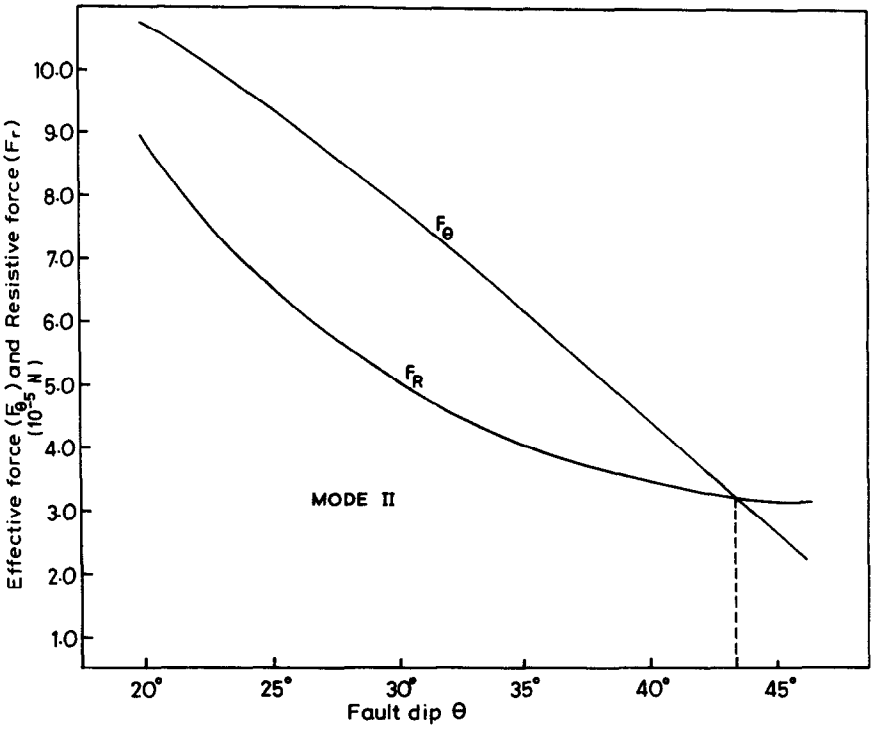

Fig. 11. Plots of effective fault-parallel force (F_θ) in a domino block and frictional resistive force (F_r) vs initial fault-dip (θ). Dashed line indicates the upper limit of θ below which Mode II occurs.

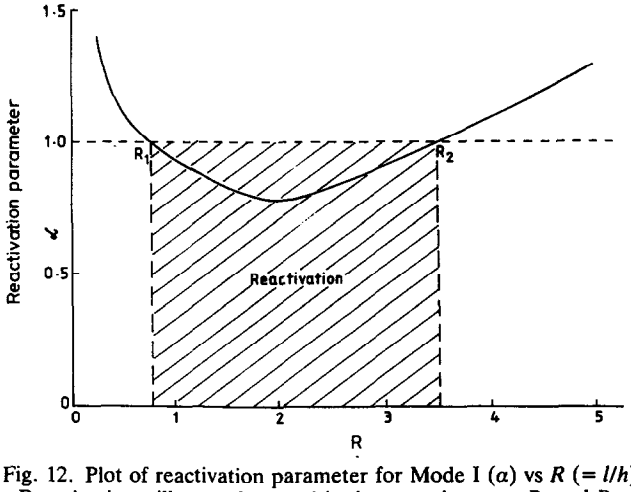

Fig. 12. Plot of reactivation parameter for Mode I (α) vs R ($= l/h$). Reactivation will occur for $\alpha < 1$ in the range between R_1 and R_2.

$$\alpha = \frac{\frac{1}{2}}{(1 + S_r) - (1 + S_r)\cos 2\theta} \frac{S_r}{R \tan \theta} \frac{(1 + R \tan \theta)^2}{} + \lambda\{\mu(1 - \tfrac{1}{2}\sin 2\theta) \tan \theta\} \quad (2)$$

where $R = l/h$.

If $\alpha < 1$, the domino system will be unstable due to fault-block counter-rotation. Therefore, normal faults can reactivate in Mode I only when the geometrical factors R and θ and the stress factor (S_r) in the contraction yield $\alpha < 1$ in equation (2). For constant values of θ (=50°) and S_r (=0.33), equation (2) shows a nonlinear variation of α with R (Fig. 12). The α vs R curve intersects the line $\alpha = 1$ at two points R_1 and R_2. Only those domino structures with $R_1 < R < R_2$ are mechanically favoured for Mode I.

Mode II: Similarly, a parameter, β, for Mode II can be generated using the ratios between resistive forces and driving forces as

$$\beta = \psi_1 + \lambda\psi_2 \quad (3)$$

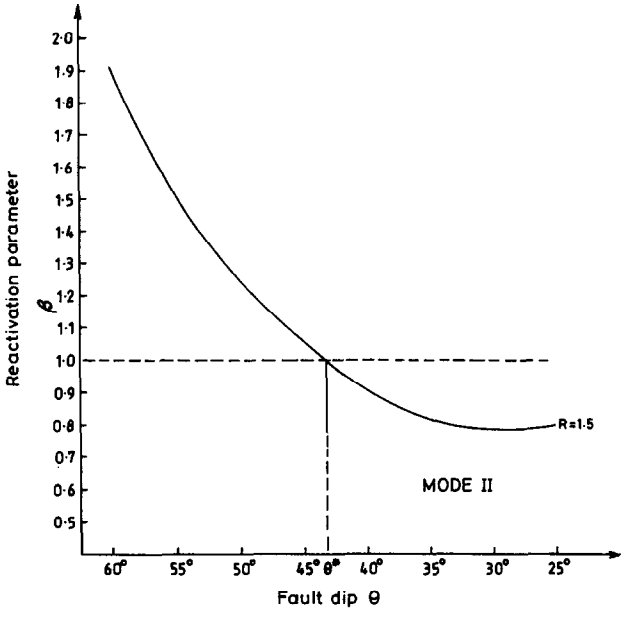

Fig. 13. Plot of reactivation parameter for Mode II (β) vs initial fault dip (θ). θ^* is the critical value below which Mode II operates.

where $\psi_1 = F_2/F_1$ and $\psi_2 = F_r/F_1$. Substituting ψ_1 and ψ_2 from equations (A20) and (A21) in equation (3),

$$\beta = \frac{S_r}{1 - S_r} R \tan \theta + \lambda\mu\left(\frac{1 + S_r}{1 - S_r} - \cos 2\theta\right) \times \frac{1 - (R/2)\sin 2\theta}{\sin 2\theta}. \quad (4)$$

Normal faults can be reactivated in Mode II when the geometric factors (R, θ) and stress factor (S_r) yield $\beta < 1$ in equation (4). β is most sensitive to fault dip (θ). The critical angle below which Mode II becomes significant is $\theta^* = 43°$ (Fig. 13) when $R = 1.5$, $S_r = 0.33$ and $\mu = 0.6$.

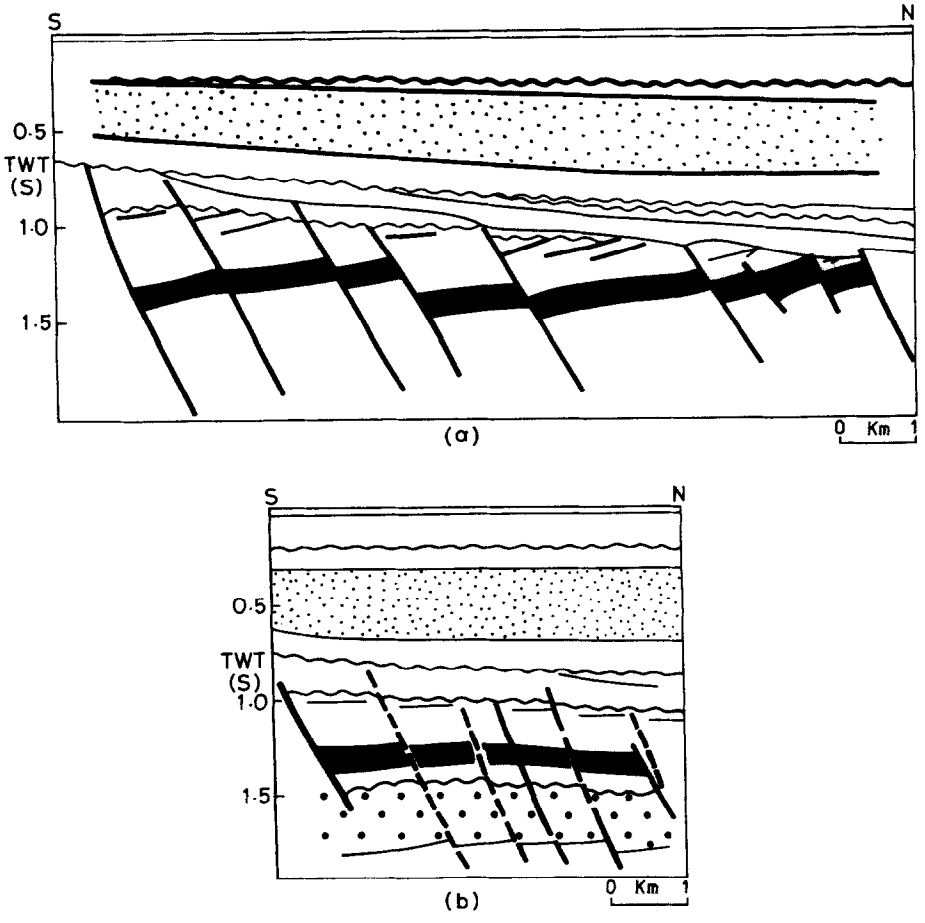

Fig. 14. Line drawings from seismic sections showing inversion structures north (a) and south (b) of the South Hewett Fault, southern North Sea. Sections show fault offsets at the Top Zechstein and Top Rotligend (thick solid band). (After Badley *et al.* 1989, reproduced with permission of Blackwell Science Ltd.)

The Mode II of reactivation can operate if normal faults have rotated significantly during the first extension episode to dips lower than the critical angle.

DISCUSSION AND CONCLUSION

Experiments show that reverse reactivation of normal faults is greatly controlled by their initial arrangement. Normal faults in extensional areas have various arrangements and will therefore respond very differently to later superimposed contraction. Depending upon the initial fault dip, parallel (domino) faults can be reactivated either in Mode I or Mode II. For example, in the southern North Sea (fig. 2, Badley *et al.* 1989) normal faults, north of the South Hewett Fault (Fig. 14a) have gentle dips and locally show offset of the top Zechstein and Rotliegend, although the beds are inclined, as seen in Mode II (Fig. 6c). In contrast, parallel faults south of the South fault zone (Fig. 14b) are relatively steeper and the same stratigraphic units are horizontal and show no significant offset, which is similar to Mode I inversion structures (Figs. 6b and 7a).

The present analysis may help to explain fault geometries on seismic profiles in areas of inversion tectonics. Assuming a bed thickness (h) of, say 6 km. Figure (12) indicates that reactivation occurs for a bed thickness–fault spacing ratio, R, = 0.8–3.5. In the domains with large fault spacing, say 12 km, the faulted horizon will be restored significantly and somewhere the initial fault offsets may not be observed in the seismic profiles. On the other hand, seismic profiles may show significant offsets and tilts of stratigraphic units where fault spacing were initially larger than 21 km. Reactivation is also not favoured for $R < 0.8$. Normal faults with low initial spacing, say 3 km, are likely to undergo selective reactivation during tectonic inversion leading to variable fault offsets in that domain. Again, depending upon initial fault dip Mode II may be important causing reversal offsets in the seismic profiles.

In our theoretical analysis, we did not consider the role of shear strength of intact rock. If the shear strength is higher than the theoretically derived differential stress, contraction will lead to reverse reactivation. Otherwise, the rock will fail along new thrusts while the normal faults will remain passive. During each experiment we observed a gradual change in the cohesive strength of sand–cement bed. Such a strength increase in the experiments would favour reactivation of old faults rather than formation of new faults. The theoretical analysis is based on the geometrical and rheological characteristics of normal-faulted rocks at the time of late contraction. In our experiments, we kept an identical time interval between the first (extension) and second (contraction) steps of deformation and more or less similar rheology at the onset of the late contraction.

In experiments there was a ductile base of putty. The putty was very soft and viscous forces did not significantly affect rigid motion on overyling fault blocks. The viscous putty only accommodated displacements in the faulted horizon. The motion in domino blocks due to contraction was determined by their own geometry. This suggests that a set of normal faults overlying a décollement horizon could be reactivated in a similar manner and the mode of reactivation would be determined by the domino geometry.

Experiments on large-scale faulting are conventionally conducted with non-cohesive dry sand so that the models are properly scaled to nature (McClay & Ellis 1987). In our experiments we added cement to sand in order to gain a cohesive strength in the sand bed. The cohesion was required for fault blocks to retain their shape during rigid-body rotation. The cohesive strength was in the range of $3.3–4.4 \times 10^3$ Pa. The model material is, however, geologically relevant because the material strength was fairly low with respect to the stresses that acted in model. The strength is closely compatible to the model length ratio, which was chosen 10^{-3} for convenience. But our model did not deform solely under its own weight nor had vertical stress gradient. These factors set constraints to quantitative extrapolation of our experimental results to large scale or crustal scale structures that require experiments with an account for gravity forces.

Acknowledgements—We wish to thank Prof. S. K. Ghosh for his suggestions in course of the present work. We also thank Dr J. P. Evans for giving us an outline in revising the manuscript. Dr B. Vendeville and Dr F. Dula reviewed the manuscript critically and suggested several modifications to upgrade the paper. The DST, India and Jadavpur University provided financial assistance for the present work.

REFERENCES

Allmendinger, R. W., Hauge, T. A., Hauser, E. C., Pottr, C. J., Klemperer, S. L., Nelson, K. D., Kneupfer, P. & Oliver, J. 1987. Overview of the COCORP 40 N Transect, western United States: the fabric of an orogenic belt. *Bull. geol. Soc. Am.* **98**, 309–319.

Badley, M. E., Price, J. D. & Backshall, L. C. 1989. Inversion, reactivated faults and related structures: seismic examples from the southern North Sea. In: *Inversion Tectonics* (edited by Cooper, M. A. & Williams, G. D.). *Spec. Publ. geol. Soc.* **44**, 201–219. Blackwell Scientific Publ., Oxford.

Brewer, J. A. & Smythe, D. K. 1984. MOIST and the continuity of crustal reflector geometry along the Caledonian–Appalachian orogen. *J. Geol. Soc. Lond.* **141**, 105–120.

Bruhn, R. L. & Dalziel, W. D. 1977. Destruction of early Cretaceous marginal basin in the Andes of Tierra del Fuego. In: *Maurice Ewing Series*, 1, *Island Arc, Deep Sea Trenches And Back-Arc Basins* (edited by Talwani, M. & Pitman, W. J. III). 395–406.

Butler, R. W. H. 1989. The influence of pre-existing basin structure on thrust system evolution in the Western Alps. In: *Inversion Tectonics* (edited by Cooper, M. A. & Williams, G. D.), *Spec. Publ. geol. Soc.* **44**, 105–122. Blackwell Scientific Publ., Oxford.

Célérier, B. 1988. How much does slip on a reactivated fault plane constrain the stress tensor? *Tectonics* **7**, 1257–1278.

Cooper, M. A. & Williams, G. D. (eds). 1989. *Inversion Tectonics. Spec. Publ. geol. Soc.* **44**. Blackwell Scientific Publ., Oxford.

Doser, D. I. 1987. The Ancash, Peru, earthquake of 1946, November 10: evidence for low angle normal faulting in the high Andes of Northern Peru. *Geophys. J. R. astr. Soc.* **91**, 57–71.

Enfield, M. A. & Coward, M. P. 1987. The structure of the West Orkney Basin, northern Scotland. *J. geol. Soc. Lond.* **144**, 871–884.

Etheridge, M. A. 1986. On the reactivation of extensional fault systems. *Phil. Trans. R. Soc. Lond.* **A317**, 179–194.

Graciansky de, P. C., Dardeau, M. L., Lemoine, M. & Tricart, P. 1989. The inverted margin of the French Alps and foreland basin inversion. In: *Inversion Tectonics* (edited by Cooper, M. A. & Williams, G. D.). *Spec. Publ. geol. Soc.* **44**, 87–104. Blackwell Scientific Publ., Oxford.

Hatcher, R. D. Jr. 1981. Thrusts and nappes in the Northern American Appalachian Orogen. In: *Thrust and Nappe Tectonics* (edited by McClay, K. R. & Price, N. J.). Blackwell Scientific Publications, Oxford, 495–499.

Ivins, E. R., Dixon, T. H. & Golombek, M. P. 1990. Extensional reactivation of an abandoned thrust: a bound on shallowing in the brittle regime. *J. Struct. Geol.* **12**, 303–314.

Letouzey, J., Werner, P. & Marty, A. 1990. Fault reactivation and structural inversion. Backarc and intraplate compressive deformations. Example of the eastern Sunda shelf (Indonesia). *Tectonophysics* **183**, 341–362.

McClay, K. R. 1989. Analogue models of inversion tectonics. In: *Inversion Tectonics* (edited by Cooper, M. A. & Williams, G. D.). *Spec. Publ. geol. Soc.* **44**, 41–59. Blackwell Scientific Publ., Oxford.

McClay, K. R. & Buchanan, P. G. 1991. Thrust faults in inverted extensional basins. In: *Thrust Tectonics* (edited by McClay, K. R.). Chapman & Hall, London, 93–104.

McClay, K. R. & Ellis, P. G. 1987. Analogue models of extensional fault geometries. In: *Continental Extensional Tectonics* (edited by Coward, M. P., Dewey, J. F. & Hancock, P. L.). *Spec. Publ. geol. Soc.* **28**, 109.125. Blackwell Scientific Publ., Oxford.

McClay, K. R., Insley, M. R. & Anderton, R. 1989. Inversion of the Kechika Trough, Northeastern British Columbia, Canada. In: *Inversion Tectonics* (edited by Cooper, M. A. & Williams, G. D.). *Spec. Publ. geol. Soc.* **44**, 235–257. Blackwell Scientific Publ., Oxford.

Muskhelishvili, N. I. 1953. *Some Basic Problems of Mathematical Theory of Elasticity*. Noordhoff, Groningen, The Netherlands.

Smith, R. B. & Bruhn, R. L. 1984. Interplate extensional tectonics of the eastern Basin–Range: inferences on structural style from seismic reflection data, regional tectonics and thermal–mechanical models of brittle-ductile deformation. *J. geophys. Res.* **89**, 5733–5762.

Sykes, L. R. 1978. Interplate seismicity, reactivation of pre-existing zones of weakness, alkaline magmatism and other tectonism postdating continental fragmentation. *Rev. Geophys. & Space Phys.* **16**, 621–687.

Vendeville, B., Cobbold, P. R., Dary, P., Brun, J. P. & Choukroune, P. 1987. Physial models of extensional tectonics at various scales. In: *Continental Extensional Tectonics* (edited by Coward, M. P., Dewey, J. F. & Hancock, P. L.). *Spec. Publ. geol. Soc.* **28**, 95–107. Blackwell Scientific Publ., Oxford.

Wernicke, B. 1981. Low-angle normal faults in the Basin and Range province: nappe tectonics in an extending orogen. *Nature* **291**, 645–648.

Wernicke, B., Walker, J. D. & Beaufait, M. S. 1985. Structural discordance between Neogene detachments and frontal Sevier thrusts, central Mormon Mountains, southern Nevada. *Tectonophysics* **4**, 213–246.

Williams, G. D., Powell, C. M. & Cooper, M. A. 1989. Geometry and kinematics of inversion tectonics. In: *Inversion Tectonics* (edited by Cooper, M. A. & Williams, G. D.). *Spec. Publ. geol. Soc. Lond.* **44**, 3–15.

APPENDIX

The normal and tangential components of the traction to a surface element are

$$T_n = F_n \, ds \tag{A1a}$$

$$T_f = F_f \, ds \tag{A1b}$$

where F_n and F_f are forces per unit area perpendicular and parallel to the fault face, respectively. The moment at any point (x',y') on fault face F_2 (Fig. 8) due to the action of T_n is

$$dm = F_n \, dx' \, x' \tag{A2}$$

The total moment is obtained by integrating equation (A2) as

$$M_d = \int_{x_1'}^{x_2'} F_n \, dx' \, x' \tag{A3}$$

$$M_d = F_n \frac{x_2'^2 - x_1'^2}{2}. \quad \text{(A4)}$$

From Fig. 8 we have,

$$x_1' = h \operatorname{cosec} \theta - l \cos \theta \quad \text{(A5a)}$$

$$x_2' = h \operatorname{cosec} \theta + l \cos \theta. \quad \text{(A5b)}$$

Substituting x_1' and x_2' in equation (A4) and after simplification,

$$M_d = 2 F_n (h) (l) \cot \theta. \quad \text{(A6)}$$

Let σ_1 and σ_3 be principal stresses in contractional deformation, where σ_1 is the horizontal compressive stress, perpendicular to the fault-strike and σ_3 is the vertical stress. Then F_n can be expressed as

$$F_n = \frac{\sigma_1 + \sigma_3}{2} - \frac{\sigma_1 - \sigma_3}{2} \cos 2\theta. \quad \text{(A7)}$$

Substituting F_n in equation (A6) we get

$$M_d = \{(\sigma_1 + \sigma_3) - (\sigma_1 - \sigma_3) \cos 2\theta\} (h) (l) \cot \theta$$

$$= \sigma_1 \{(1 + S_r) - (1 - S_r) \cos 2\theta\} (h) (l) \cot \theta \quad \text{(A8)}$$

where $S_r = \sigma_3/\sigma_1$.

The opposing moment in the block due to the downward vertical force on the faulted horizon is

$$M_v = \int_0^{x_2} \sigma_3 \cdot dx \cdot x$$

$$= \sigma_3 \frac{x_2^2}{2}$$

where (x_2, y_2) is the co-ordinate of P_2 with respect to the xy-frame (Fig. 8). Since

$$x_2 = l + h \cot \theta,$$

$$M_v = \frac{(l + h \cot \theta)^2}{2} \sigma_3 \quad \text{(A9)}$$

the effective moment in the block, resulting from M_d and M_v in equations (A8) and (A9), is

$$M_r = \sigma_1 \left[\{(1 + S_r) - (1 - S_r) \cos 2\theta\} h l \cot \theta - S_r \frac{(l + h \cot \theta)^2}{2} \right]. \quad \text{(A10)}$$

In response to the action of M_r rotational motion will occur in the block when the frictional resistance along the fault planes is overcome. The reactive forces act from 0 to x_1. As fricitonal force is directly proportional to the reactive force, the total frictional resistance is $2 F_n \mu (h \operatorname{cosec} \theta - l \cos \theta)$, where μ is co-efficient of friction on the fault. The opposing moment due to the frictional force is

$$M_f = 2 \mu F_n (h \operatorname{cosec} \theta - l \cos \theta) l \sin \theta. \quad \text{(A11)}$$

By substituting F_n from equation (7),

$$M_f = 2\mu \left(\frac{\sigma_1 + \sigma_3}{2} - \frac{\sigma_1 - \sigma_3}{2} \cos 2\theta \right) (h \operatorname{cosec} \theta - l \cos \theta) l \sin \theta$$

$$M_f = \mu \sigma_1 \{(1 + S_r) - (1 - S_r) \cos 2\theta\} (h - \tfrac{1}{2} l \sin 2\theta) l. \quad \text{(A12)}$$

The tangential traction per unit area on the fault is

$$F_f = \frac{\sigma_1 - \sigma_3}{2} \sin 2\theta. \quad \text{(A13)}$$

By substituting F_f in equation (A1b) and integrating the equation, the total tangential force is

$$F_t = \int_{-x_2'}^{x_2'} \left(\frac{\sigma_1 - \sigma_3}{2} \sin 2\theta \right) dx'$$

$$F_t = \frac{\sigma_1 - \sigma_3}{2} \sin 2\theta \, 2x_2'.$$

From Fig. 8

$$x_2' = h \operatorname{cosec} \theta$$

then

$$F_t = (\sigma_1 - \sigma_3) h \operatorname{cosec} \theta \sin 2\theta$$

$$F_t = 2\sigma_1 (1 - S_r) h \cos \theta \quad \text{(A14)}$$

The downward force in the block is $2\sigma_3 l$. The fault-parallel component of this force is

$$F_d = 2\sigma_3 l \sin \theta. \quad \text{(A15)}$$

From equations (A14) and (A15), the resultant force that induces fault slip is

$$F_\theta = 2\sigma_1 \{(1 - S_r) h \cos \theta - S_r l \sin \theta)\}. \quad \text{(A16)}$$

The frictional resistance to the block is

$$F_R = \mu \sigma_1 \{(1 + S_r) - (1 - S_r) \cos 2\theta\} (h \operatorname{cosec} \theta - l \sin \theta). \quad \text{(A17)}$$

From equations (A8) and (A9), the ratios of opposing moments to the driving moment in the block are

$$\phi_1 = \frac{\frac{1}{2}\sigma_3 (l + h \cot \theta)^2}{\sigma_1 \{(1 + S_r) - (1 - S_r) \cos 2\theta\} h l \cot \theta}$$

$$= \frac{\frac{1}{2} S_r (h + l \tan \theta)^2}{l.h \{(1 + S_r) - (1 - S_r) \cos 2\theta\} \tan \theta}$$

$$= \frac{\frac{1}{2} S_r (1 + R \tan \theta)^2}{\{(1 + S_r) - (1 - S_r) \cos 2\theta\}.R \tan \theta} \quad \text{(A18)}$$

and

$$\phi_2 = \frac{2\mu (h \operatorname{cosec} \theta - l \cos \theta) \sin \theta}{2 h \cot \theta}$$

$$= \frac{\mu (h - \frac{1}{2} l \sin 2\theta) \tan \theta}{h}$$

$$= \mu (1 - \tfrac{1}{2} R \sin 2\theta) \tan \theta. \quad \text{(A19)}$$

From equations (A14), (A15) and (A16), the ratios of resistive forces to the driving force are

$$\psi_1 = \frac{\sigma_3 l \sin \theta}{(\sigma_1 - \sigma_3) h \cos \theta}$$

$$= \frac{S_r}{1 - S_r} R \tan \theta \quad \text{(A20)}$$

and

$$\psi_2 = \frac{\mu \sigma_1 \{(1 + S_r) - (1 - S_r) \cos 2\theta\} \{h \operatorname{cosec} \theta - l \cos \theta\}}{2\sigma_1 (1 - S_r) h \cos \theta}$$

$$= \mu \left(\frac{1 + S_r}{1 - S_r} - \cos 2\theta \right) \left(\frac{1 - \frac{R}{2} \sin 2\theta}{\sin 2\theta} \right). \quad \text{(A21)}$$